Missouri University of Science and Technology

Scholars' Mine

International Conference on Case Histories in Geotechnical Engineering

(2008) - Sixth International Conference on Case Histories in Geotechnical Engineering

14 Aug 2008, 2:15pm - 4:00pm

Evolution of Soil Desaturation by Air-Injection Technique and Its Evaluation via Multiphase Flow Simulation

Hide Yasuhara
Ehime University, Matsuyama, Japan

Takamasa Morito
Fudo Tetra Corporation, Chiba, Japan

Yoshinori Kochi
Ehime University, Matsuyama, Japan

Mitsu Okamura
Ehime University, Matsuyama, Japan

Recommended Citation

EVOLUTION OF SOIL DESATURATION BY AIR-INJECTION TECHNIQUE AND ITS EVALUATION VIA MULTIPHASE FLOW SIMULATION

Hide Yasuhara
Ehime University
Matsuyama, Japan

Takamasa Morito
Fudo Tetra Corporation
Chiba, Japan

Yoshinori Kochi
Ehime University
Matsuyama, Japan

Mitsu Okamura
Ehime University
Matsuyama, Japan

ABSTRACT

In this study the simplified model tests that simulate air injection into saturated soils using air-injection probes, are conducted using the two different sizes of soil containers. The experiments using the small container are aimed to examine the rates and magnitudes of the soil desaturation driven by air injection, whilst those with the large container are performed to obtain not only the rates and magnitudes but also the distributions of the desaturated zones within the soil, and to examine influences on the desaturation process exerted by anisotropy of the soil in terms of flow transport. Obtained results indicate that the evolution of desaturation is strongly controlled by the soil permeabilities.

Numerical analyses are also conducted using a multiphase flow simulator to describe the evolution of the soil desaturation, and to examine an applicability of the model as a prediction tool enabling an evolution of desaturation *in situ* to be followed with time and space. Predictions show a relatively good agreement with the measurements regarding the rates, magnitudes, and distribution of desaturation although predictions of the airflow rates underestimate the measurements for both small- and large-container experiments, and in the large container the early periods of the experiments are ill-replicated by the model.

INTRODUCTION

Measures preventing an earthquake-induced soil liquefaction are of significant importance to mitigate the liquefaction hazards. Improving the strength, density, and drainage characteristics of the soils is one of the most popular methods to reduce the liquefaction susceptibility. For instance, dynamic compaction, compaction grouting, and drainage techniques may be widely applied for the purpose, but their installation costs are generically expensive.

An air-injection technique [Okamura and Teraoka, 2005; Okamura and Soga, 2006] may be a simple, inexpensive alternative – this leads the saturated soils to the desaturated by injecting pressurized air bubbles, resulting in a higher liquefaction strength and the lower susceptibility. As experimental evidences of lowering liquefaction susceptibility induced by desaturation, Yoshimi et al. [1989] have conducted cyclic torsional shear tests and concluded that a soil specimen shows threefold liquefaction resistance ratio as the saturation decreases from fully-saturated to 70 %. To evaluate an augmentation in liquefaction resistance via soil desaturation by air injection, the rates, magnitudes, and distributions of the desaturation should be obtained, *a priori*. In the field of air-sparging for subsurface remediation, mathematical modelings and numerical simulations are popular to predict behavior of a multiphase flow within soils [Lundegard and Andersen, 1996; McCray, 2000; Tsai, 2007]. Specifically, McCray [2000] have reviewed the existing mathematical models describing the behavior moderated by air sparging and concluded that the multiphase flow models might be very useful to describe a desaturation process induced by air sparging as long as detailed model calibration is well-conducted.

In this study, desaturation experiments utilizing air-injection probes are conducted using the two different sizes of soil containers. The experiments with the small container are to examine the rates and magnitudes of soil desaturation driven by air injection, whereas those with the large are to obtain not only the rates and magnitudes but also the distributions of the desaturated zones within the soil, and to examine influences on the desaturation process exerted by anisotropy of the soil with different permeabilities in vertical and horizontal directions. We also attempt to predict the measured desaturation processes both during air injection and after the injection is halted, using a multiphase flow simulator for the both experiments and examine a validity of the simulator if this is capable of being applied to real sites.

EXPERIMENTS

A desaturation process within soils via air injection is examined using the two different sizes of containers as shown in Fig. 1. The small container is relatively simple to conduct experiments – preparing model grounds is straightforward due to the smaller volume and an average saturation is measured within a whole domain, but have a limitation that horizontal expansion of air bubbles may be interfered by side walls. Whereas the large container has several advantages that the sufficiently wide side-walls never hinder airflows, and local saturations are measured by TDR probes inserted within the container. However, preparing model grounds is relatively laborious because of its bulk, and it has a potential against boiling sand as overburden pressure may not be applied equivalently on the top of grounds. Both experiments are explained in details in the following sections.

Experimental measurements with small container

The small container (Fig. 1a) is made of acrylic boards with a internal dimension of 77 cm height, 25 cm width, and 10 cm depth. A fully saturated 30 cm-height model ground is constructed in such a way that dry Toyoura sand is rained in water and compacted every 5 – 8 cm height to have a relative density of 60 %. After constructed, an overburden pressure of 40 kPa is applied on the top of the ground to prevent the soil from boiling and piping mediated by air injection. A water pressure gage is installed above the model ground to measure continuously evolution of the water level induced by air injection. Thus, an average degree of saturation within the model ground may be simply evaluated as,

$$S_a = 1 - \frac{\Delta h}{h_s \cdot \phi} , \qquad (1)$$

where Δh represents the change of water level from the initial. h_s is the height of the model ground, and ϕ is the porosity.

Air injection with air pressure of 12 kPa is conducted. Once injected, air dominantly flows in horizontal direction, and moves upwards after reaching the side walls, indicating that the horizontal permeability is greater than the vertical. The evolution of degree of saturation by air injection, together with change of airflow rates with time, is depicted in Fig. 2. As apparent, firstly the degree of saturation monotonically decreases with time and then reaches steady state with the saturation of 64 %. Similarly, the flow rate increases with time up to the steady value of 52 cm^3/sec. This implicates that ultimate degrees of saturation and flow rates are controlled by air pressure at the inlet. After the temporal steady state, the air injection is halted. Subsequently, the saturation gradually
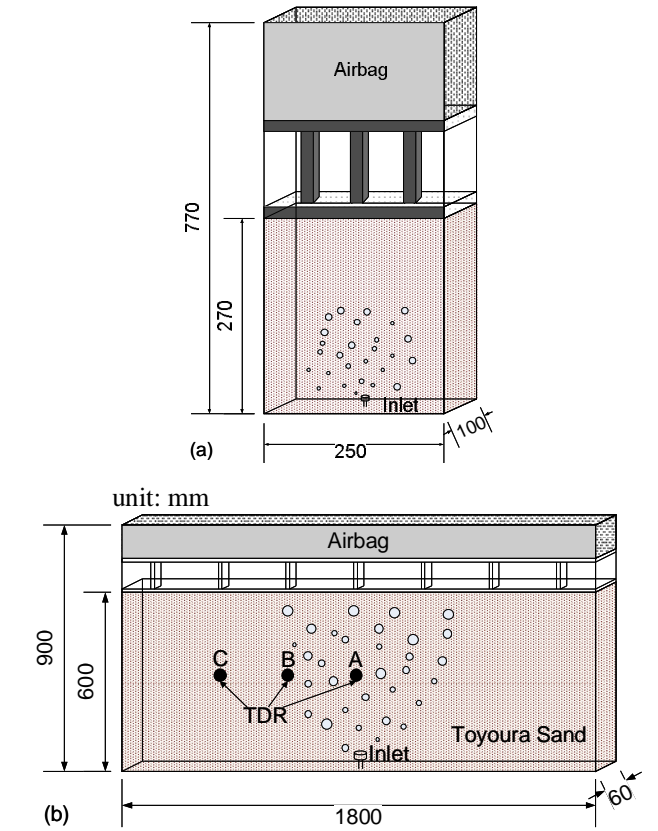

Fig. 1. Schematic of the two experimental containers ((a) the small container and (b) the large container). For the large container, local saturations are measured by TDR probes.
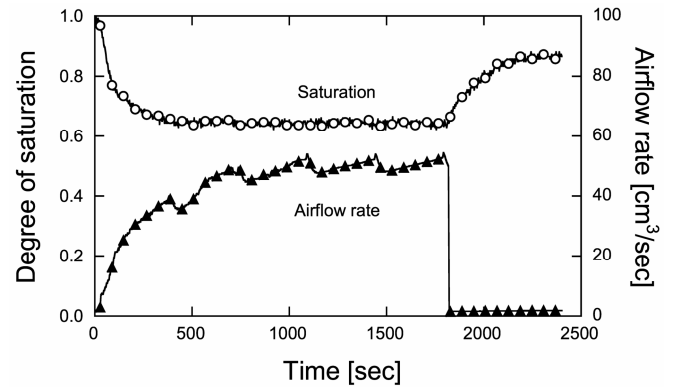

Fig. 2. Changes in degree of saturation and airflow rate with time for the small-container experiments.

increases with time and recovers up to 85 %, but never reaches the fully-saturated due to residual air trapped within pore spaces.

Experimental measurements with large container

The large container (90 cm height×172 cm width×6 cm depth) is also made of acrylic boards and significantly wider than the small. Thus, airflow is not hindered by the side walls.

Moreover, local saturations are measurable using TDR probes at the three locations (A), (B), and (C) (Fig. 1b). The model ground is constructed by the same way as the small container, and the final height of the ground is 60 cm. This ground is also pressurized by an overburden pressure of 50 kPa.

Instead of a constant air pressure for air injection as the previous attempts, the air pressures are increased step by step from 8 – 15 kPa as shown in Fig. 3a. The airflow rate increases with increase in air pressure (Fig. 3b), whereas the degrees of saturation at the locations (A) and (B), following the sharp reductions in the early periods, slightly evolves with time (Fig. 3c). Note that flow around the location (C) may be stagnant and the soil keeps fully-saturated throughout the experiments in resulting from the airflow never reaches there. Once air injection halted, the degrees of saturation at (A) and (B) suddenly increase up to ~85 %.

Experimental measurements with small and large containers show a desaturation process mediated by air injection to be followed with time (and space only for the large-container experiments). This well-presented results are attempted to be replicated by a multiphase flow predictions, that is explaining in the following chapter.

NUMERICAL SIMULATION OF MULTIPHASE FLOW

Simultaneous flow of water and air occurs during air injection (i.e., desaturation process). Thus, the effects of capillary pressures and the mutual flow impedance between the two phases should be involved in the model with a theoretical assessment. In this chapter, firstly a suite of the mathematical equations used for the multiphase flow simulations is presented and then the parameters for predictions are identified through replicating column experiments for determining soil-water retention characteristics. Finally, the comparison results between the experimental measurements and the predictions are shown in detail.

Mathematical formation for multiphase flow

We use a multiphase flow simulator of TOUGH2 [Pruess et al. 1999] to describe a desaturation process and to examine an applicability of the model if replicating the experimental measurements. A mass balance may be expressed in integral form for arbitrary sub-volume, V_n, bounded by a surface area of Γ_n, given as,

$$\frac{d}{dt}\int_{V_n} M^\kappa dV_n = \int_{\Gamma_n} \mathbf{F}^\kappa \cdot \mathbf{n}\, d\Gamma_n + \int_{V_n} q^\kappa dV_n \, , \qquad (2)$$

where κ denotes the component, M^κ is the amount of component κ with a dimension of mass per volume, $\mathbf{F}^\kappa$ is the flux of component κ, $\mathbf{n}$ is the outward unit vector normal to the volume surface, q^κ is the rate of generation of component κ within the volume.
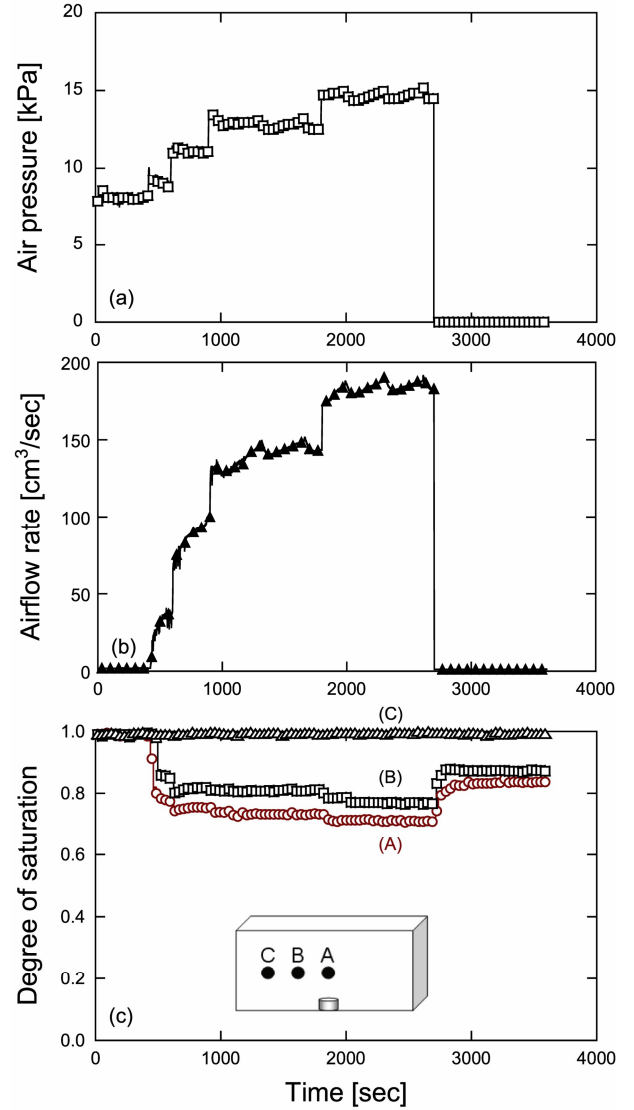

Fig. 3. Changes in (a) air pressure, (b) airflow rate, and (c) degree of saturation at the locations A, B, and C with time for the large-container experiments.

The mass accumulation term for air and water is given by,

$$M^\kappa = \phi \sum_\beta S_\beta \rho_\beta X_\beta \, , \qquad (3)$$

where S_β, ρ_β, and X_β denote the saturation, density, and mass fraction of phase β (liquid or gaseous phase), respectively. The advective mass flux terms sum over the liquid and gaseous phases, as,

$$\mathbf{F}^\kappa = \sum_\beta X_\beta^\kappa \mathbf{F}_\beta \, . \qquad (4)$$

Advective flow for each phase β is defined by considering the driving forces of pressure and gravity according to a multiphase extension of Darcy's low, given as,

$$\mathbf{F}_\beta = \rho_\beta \mathbf{u}_\beta = -k \frac{k_{r\beta} \rho_\beta}{\mu_\beta} \left(\nabla P_\beta - \rho_\beta \mathbf{g} \right), \qquad (5)$$

where $\mathbf{u}_\beta$ is the β phase Darcy velocity, k is the intrinsic permeability, $k_{r\beta}$ is the β phase relative permeability, μ_β is the β phase dynamic viscosity, P_β is the β phase pressure, and $\mathbf{g}$ is the gravitational acceleration vector. The Zunker empirical formula is employed to obtain intrinsic permeability. The formula that gives hydraulic conductivity, takes the form as,

$$K = C_z \frac{g}{v_w} \left(\frac{\phi}{1-\phi} \right)^2 D_w^2, \qquad (6)$$

where K is the hydraulic conductivity, C_z is the empirical coefficient based on porosity, v_w is the kinematic viscosity for water, and D_w is the effective grain diameter. The intrinsic permeability, k, is obtained by the following relation between K and k, given as,

$$k = \frac{v_w}{g} K, \qquad (7)$$

The Mualem-van Genuchten model [Mualem, 1976; van Genuchten, 1980] is used to describe the relation between saturation and β phase relative permeability, as,

$$k_{rl} = \begin{cases} \sqrt{S^*} \left\{ 1 - \left(1 - [S^*]^{1/\lambda} \right)^\lambda \right\}^2 & \text{if } S_l < S_{ls} \\ 1 & \text{if } S_l < S_{ls} \end{cases}, \qquad (8)$$

$$k_{rg} = \begin{cases} 1 - k_{rl} & \text{if } S_l < S_{ls} \\ \left(1 - \hat{S} \right)^2 \left(1 - \hat{S}^2 \right) & \text{if } S_l < S_{ls} \end{cases}, \qquad (9)$$

where,

$$S^* = \left(S_l - S_{lr} \right) / \left(S_{ls} - S_{lr} \right), \qquad (10)$$

$$\hat{S} = \left(S_l - S_{lr} \right) / \left(1 - S_{lr} - S_{gr} \right). \qquad (11)$$

Here, S_{ls} is the maximum liquid saturation, and λ is the constant. S_{lr} and S_{gr} denote the residual liquid and gaseous saturation, respectively.

The relation between liquid (l) and gaseous (g) pressures is defined, via the capillary pressure, P_{cap}, as,

$$P_l = P_g + P_{cap}. \qquad (12)$$

The relation between the capillary pressure and saturation (i.e., water retention curve) may be described by the van Genuchten equation [van Gennuchten, 1980], as,

$$P_{cap} = -P_0 \left([S^*]^{-1/\lambda} - 1 \right)^{1-\lambda}, \qquad (13)$$

where P_0 is the constant that may be related to an air entry value.

The continuum equations (Eq. (2)) are discretized in space to numerically solve multiphase flow processes. After discretized as a first-order finite difference, the flux and sink and source terms are evaluated at the next time step. An iterative procedure is adopted to solve in time until a prescribed time.

Fitting parametric retention and permeability functions

The relation between the capillary pressure and saturation (Eq. (13)) for the Toyoura sand utilized for the air injection experiments with the small and large containers, is determined through soil water retention experiments as shown in Fig. 4, together with the well-fitted predictions by Eq. (13). The parameters used for the fitting is tabulated in Table 1.

The parameters of λ, S_{lr}, and S_{ls} for relative permeability function (Eqs. (8)-(11)) are assumed equivalent to those determined from fitting the water retention curve for drainage. The residual gaseous saturation of S_{gr} is obtained from trapped air saturation at the end of the water retention experiment for imbibition (Table 1). The relation of relative permeability between liquid and gaseous phases with the determined values, is depicted in Fig. 5.
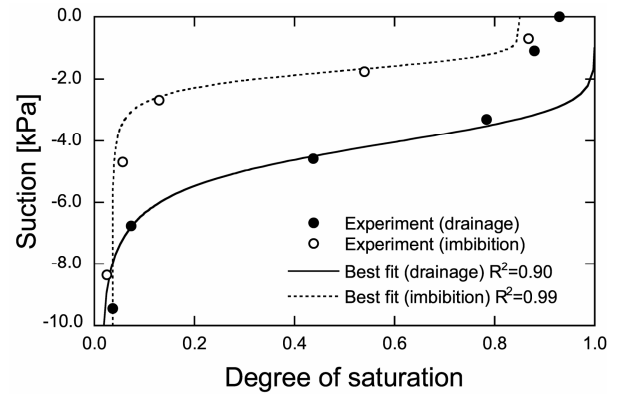

Fig. 4. Replicating experimental measurements of water retention curves for drainage and imbibition processes.

Table 1. Parameters used in the analysis (Eqs. (8)-(13)).

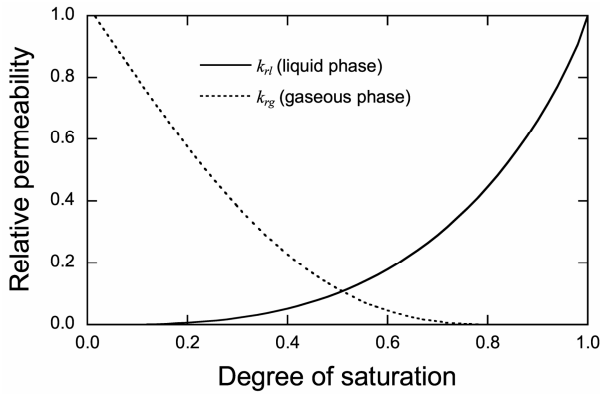| Parameters	Drainage	Imbibition
λ	0.846	0.844
P_0 [Pa]	4.15×10^3	1.74×10^3
S_{lr}	1.48×10^{-2}	3.67×10^{-2}
S_{ls}	1.00	0.849
S_{gr}	0.151	–

Fig. 5. Relative permeability for liquid and gaseous phases determined from the predictions of water retention curve for drainage.

Table 2. Parameters used in the analysis (Eqs. (6) and (7)).

Parameters	Small container	Large container
ϕ	0.41	0.46
C_z	1.5	1.5
D_w [m]	1.91×10^{-4}	1.91×10^{-4}
K [m/sec]	2.56×10^{-4}	3.61×10^{-4}
k [m^2]	2.61×10^{-11}	3.68×10^{-11}

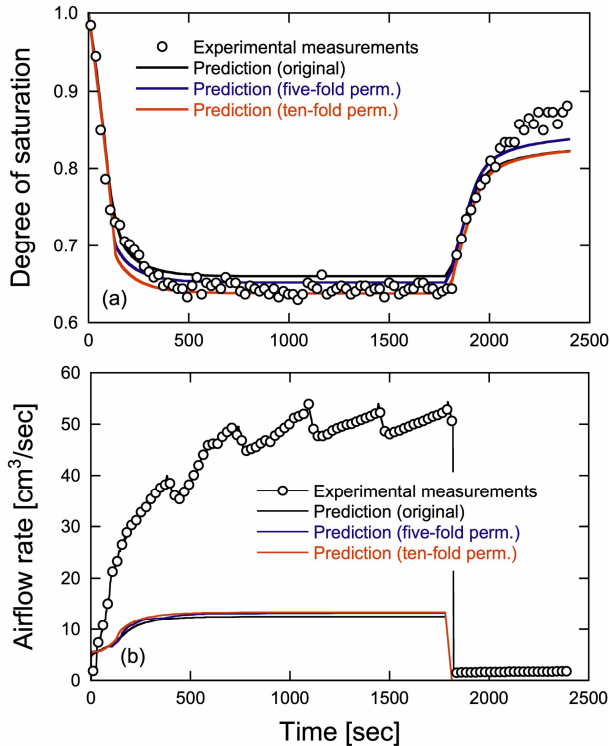Fig. 6. Comparisons between measurements and predictions with small container. (a)Degree of saturation; (b) Airflow rate.
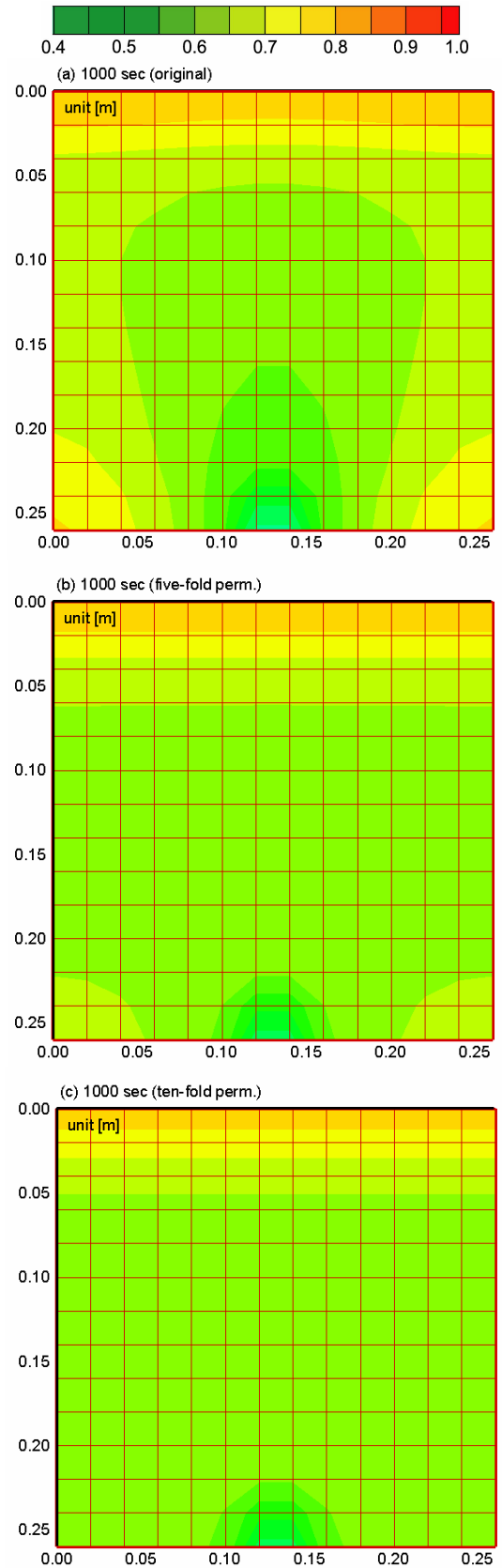

Fig. 7. Predicted distributions of degree of saturation at 1000 sec. (a)same horizontal permeability as vertical value ($k_H=k_V$); (b) $k_H=5k_V$; (c) $k_H=10k_V$.
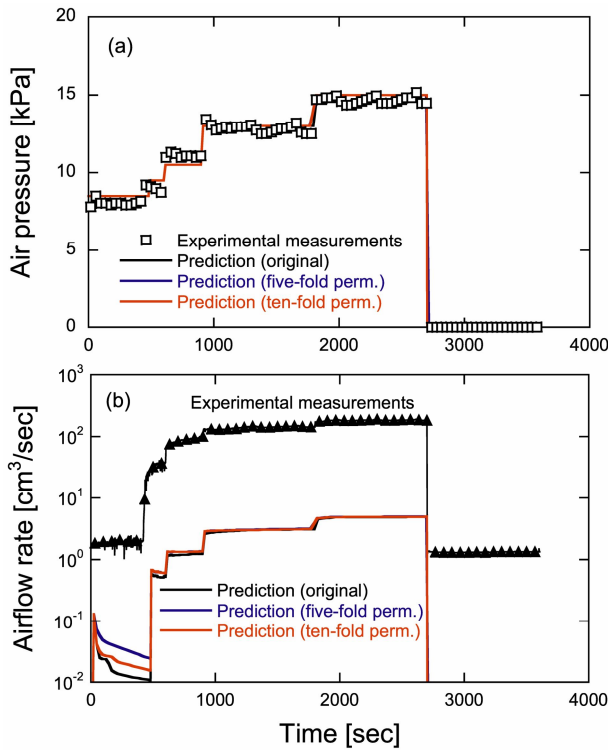
Fig. 8. Comparisons between measurements and predictions with large container. (a)Air pressure injected; (b) Airflow rate.

Fig. 9. Comparisons of degree of saturation between measurements and predictions with large container. (a)same horizontal permeability as vertical value ($k_H=k_V$); (b) $k_H=5k_V$; (c) $k_H=10k_V$.

The intrinsic permeabilities used for replicating the small- and large-container experiments are identified after constructing the both model grounds – the values of nominal porosity are evaluated based on the ground volume made and weight of sand used. The parameters utilized in the analyses are shown in Table 2.

Comparison between measurements and predictions

Firstly, desaturation processes for the small-container experiments are predicted by the model previously described. Predictions of the evolution in saturation and airflow rates with the used parameters tabulated in Table 1 and Table 2, are shown in Fig. 6, together with the experimental measurements. Generically, the horizontal permeability is thought to be greater than the vertical. Thus, predictions with the five- and ten-fold horizontal permeability based on the vertical values, are also conducted and depicted in Fig. 6. As apparent, the measured are almost situated within the predictions with the same and ten-fold horizontal permeability as the vertical, implicating that the horizontal permeability, as expected, is likely greater than the vertical. However, all predicted airflow rates underestimate the measured – roughly one-fifth of the actual. This may be attributed to the inappropriate relation between relative permeability and saturation (Fig. 5). A further investigation on the relation should be performed and it must be constrained experimentally.
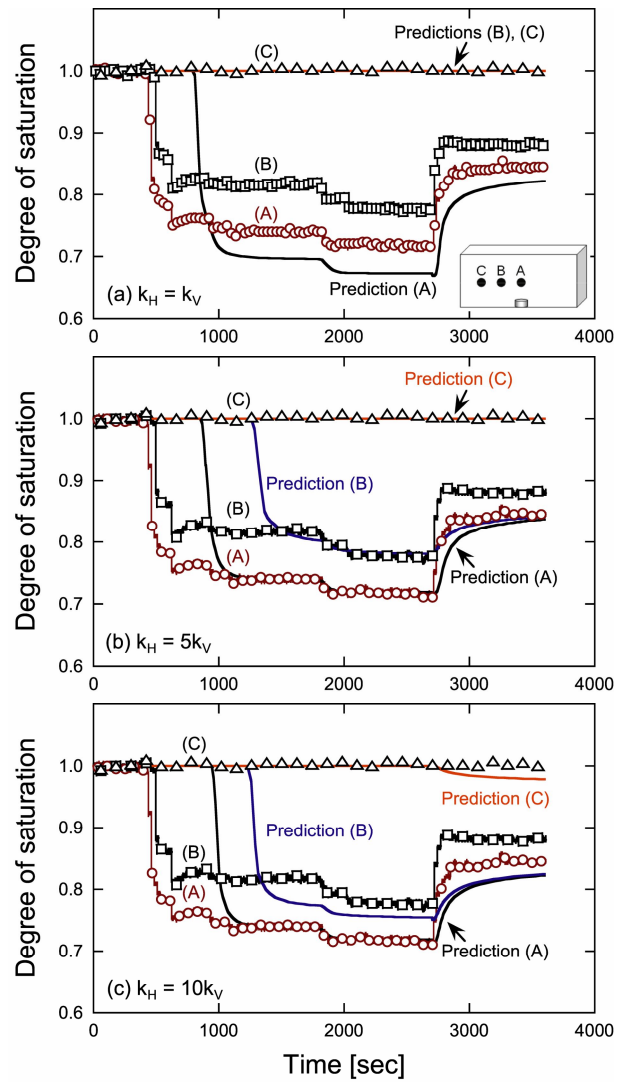
Distributions of saturation within the container can be followed with time by predictions. Those predicted at 1000 sec are depicted in Fig. 7. As apparent, the distributions are almost uniform among the three different cases although it is perceivable that air spreads more uniformly in predictions with larger permeability in horizontal direction. This implicate that the air injected reaches the sidewalls in relatively short time and ascents along them, which is consistent with visible observations during the experiments.

Fig. 8a shows the air pressure used for the predictions as boundary conditions in the large-container experiments, indicating those to be well-followed with time. Predictions in the airflow rates (Fig. 8b) significantly underestimate the measurements, as expected – roughly two orders of magnitude smaller than the actual. This may be also due to ill-identified relation between relative permeability and saturation. The

predictions with one-, five-, and ten-fold horizontal permeabilities are shown in Fig. 9. Among them, that with the five-fold horizontal permeability most closely matches with the experimental measurements. This indicates that permeability in horizontal and vertical directions should be examined and identified, in advance, before conducting *in situ* predictions.

Distributions of saturation predicted at 2500 and 3500 sec show significant dependence upon the horizontal permeability prescribed (Fig. 10 and Fig. 11) – the plumes become wider with increase in horizontal permeability. For predictions with same permeability in horizontal and vertical directions, the air injected little reaches the locations (B) and (C) at 2500 and 3500 sec, which is congruent with the actual measurements. Likewise, for the five-fold, the air does not arrive at (C) at both 2500 and 3500 sec. It is noticeable that for the ten-fold, the saturation keeps fully-saturated until 2500 sec, and the air reaches the location (C) at 3500 sec. The saturation starts to decrease as the injected is halted (Fig. 9c). This is attributed to that the air in pore spaces goes down as airflow passes expand due to the relatively high permeability in horizontal direction even when no additional air is supplied.
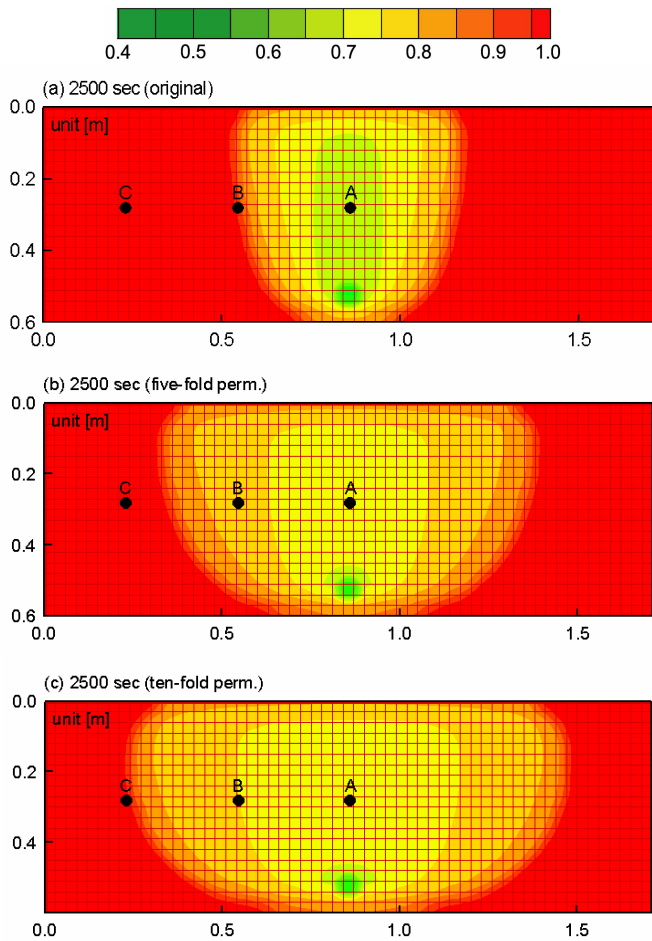
CONCLUSIONS

This work experimentally and numerically examines evolution in desaturation in terms of the rates, magnitudes, and distributions. The two different sizes of ground containers are adopted – the small-container experiments are conducted to investigate overall desaturation process, whereas those with the large container enable local desaturation processes to be followed with time using TDR probes.

In the small-container experiments with an air pressure of 12 kPa, the degrees of saturation decrease down to 64 % within a relative short time, followed by a steady state. After a shutdown of the airflow, the saturations recover to the maximum liquid saturation for imbibition (i.e., ~85 %).

In the large-container experiments local degrees of saturation are measured and show that after sharp reductions at the locations (A) and (B) those saturations stay steady although the airflow rates increase with increase in the air pressures. When the airflow is shut, the saturations abruptly increase to ~85 %, equivalent to the results in the small-container experiments.
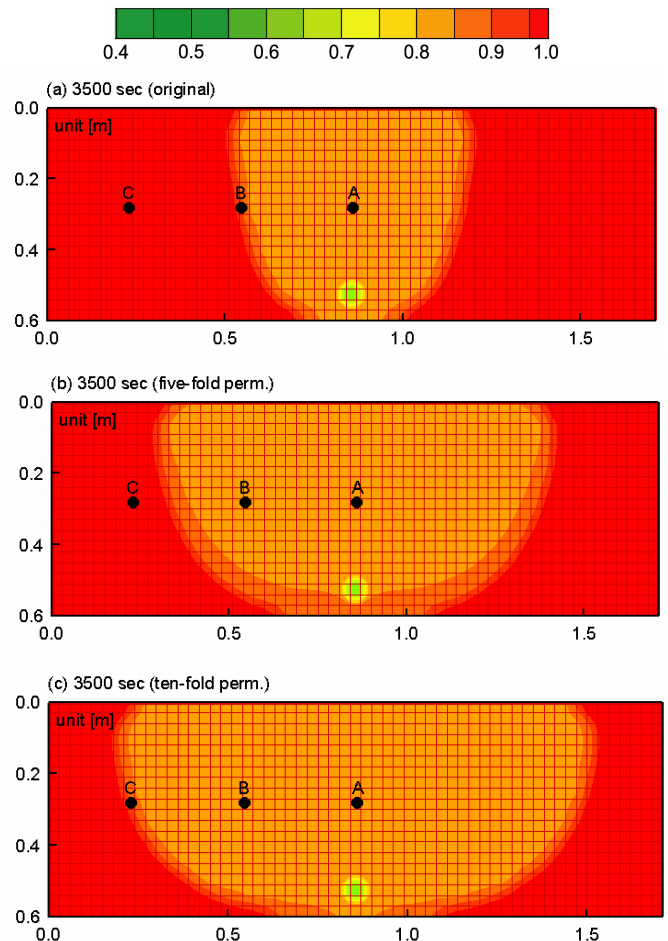

Fig. 10. Predicted distributions of degree of saturation at 2500 sec (under maximum air pressure of ~15 kPa). (a) $k_H=k_V$; (b) $k_H=5k_V$; (c) $k_H=10k_V$.

Fig. 11. Distributions of degree of saturation at 3500 sec (after air injection halted). (a) $k_H=k_V$; (b) $k_H=5k_V$; (c) $k_H=10k_V$.

Numerical simulations by a multiphase flow model show relatively good agreements with the experimental measurements of the evolution in saturations for the both small- and large-container experiments as the horizontal permeability are increased five-fold against the vertical amounts, implicating that this model may be applicable to predicting desaturation processes *in situ* to be followed with time and space. However, the airflow rates predicted significantly underestimate the actual. This may be attributed to ill-constrained relations of the relative permeability for both liquid and gas. To resolve this mismatch, a further analysis to constrain a multiphase flow mechanism (i.e., relation between liquid and gaseous relative permeabilities and saturations), is required.

REFERENCES

Lundegard, P. D. and G. Andersen [1996], "Multiphase numerical simulation of air sparging performance", *Ground Water*, Vol. 34, pp. 451-460.

McCray, J. E. [2000], "Mathematical modeling of air sparging for subsurface remediation: state of the art", *J. hazard. Mater.*, Vol. 72, pp. 237-263.

Mualem, Y. [1976], "A new model for predicting the hydraulic conductivity of unsaturated porous media", *Water Resour. Res.*, Vol. 12, pp. 512-522.

Okamura, M. and T. Teraoka [2005], "Shaking table tests to investigate soil desaturation as a liquefaction countermeasure", *ASCE Geotechnical Special Publication*, No. 145, pp. 282-293.

Okamura, M. and Y. Soga [2006], "Effect on liquefaction resistance of volumetric strain of pore fluid", *Soils Found.*, Vol. 46, pp. 703-708.

Pruess, K., C. Oldenburg, and G. Moridis [1999], "*TOUGH2 User's Guide Version 2.0*", Rep. LBNL-43134, Berkeley, CA, 197pp.

Tsai, Y. J. [2007], "Airflow paths and porosity/permeability change in a saturated zone during in situ air sparging", *J. hazard. Mater.*, Vol. 142, pp. 3157-323.

van Genuchten, M. Th. [1980], "A closed-form equation for predicting the hydraulic conductivity of unsaturated soils", *Soil Sci. Soc.*, Vol. 44, pp. 892-898.

Yoshimi, Y., K. Tanaka, and K. Tokimatsu [1989], "Liquefaction resistance of a partially saturated sand", *J. Jpn. Soc. Soil Mech. Found. Eng.*, Vol. 129, pp. 157-162.